
OPTICS
OF STOCHASTICALLY-HETEROGENEOUS MEDIA

Accuracy of Determination of Longitudinal Coordinates of Particles by Digital Holography

V. V. Dyomin^a, A. Yu. Davydova^a, I. G. Polovtsev^a, N. N. Yudin^a, *, and M. M. Zinoviev^a

^a National Research Tomsk State University, Tomsk, 634050 Russia

*e-mail: rach3@yandex.ru

Received September 1, 2022; revised October 12, 2022; accepted October 28, 2022

Abstract—Based on known expressions applied to diffraction-limited optics systems, estimates are given and a technique is suggested for determining the measurement error in the longitudinal coordinates of particles from images reconstructed from digital holograms. A correction factor for visual focusing is determined for different distances between a detected particle and the plane of a CMOS array. The results of experimental tests of the technique are presented. A possibility is shown of reducing the error of automatic digital focusing by means of simultaneous use of focusing curves for several quality indicators and optimization of the image area for their construction.

Keywords: digital particle holography, reconstructed particle images, longitudinal coordinates of particles, error, diffraction-limited systems

DOI: 10.1134/S1024856023030041

INTRODUCTION

Digital holography of particles is used in solution of many problems (mainly the axial recording scheme [1–3]) in order to detect suspended particles of different nature and determine their sizes, shapes, and coordinates [4–9]. Such particles are quite often found in different media, such as gases, liquids, and solids, and form suspensions (sols)—multiphase systems: aerosols, hydrosols, and solid sols, respectively. Examples of such particles and suspensions are: aerosol particles, droplets in a nozzle spray, plankton and other particles in sea water (sea snow, solid inorganic particles, gas bubbles, etc.), erythrocytes, void defects and inclusions in optical materials, etc.

In our previous works [4, 5, 8], we suggested the Digital Holographic Camera (DHC) technique for study of such particles. It consists of:

- recording a digital hologram of a medium volume with particles;
- numerical layer-by-layer reconstruction with a given step of the images of cross sections of the medium volume of the and fixing the longitudinal coordinate of each cross section;
- detection of cross sections which contain focused images of particles (longitudinal focusing, as in microscopy);
- determination of longitudinal and transverse coordinates, sizes, and shapes of the particles and their recognition.

This field of research is currently being actively developed [10–15]. It is not difficult to determine the transverse coordinates by finding the center of gravity of a particle image reconstructed. However, there are a few works devoted to the analysis of measurement errors in longitudinal coordinates and sizes of suspended particles by digital holography means.

Accurate positioning is required when rejecting defective materials (for example, nonlinear crystals) with inclusions (defects) when cutting them into work items.

This work is devoted to the study of the accuracy of determining the longitudinal coordinates of particles from their holographic image.

As is shown in [5] the error in the longitudinal coordinate is on the order of 100–200 μm, which is comparable and sometimes higher than the size of a particle analyzed. However, even this accuracy, which is not very high, is unattainable because of the diffraction of light at the aperture of the particle hologram and significantly depends on the distance L to the particle image reconstructed. This issue has been studied and described for diffraction-limited optical imaging systems [2, 10]. However, we have not found any works devoted to experimental studies of the effect of diffraction uncertainty of an image on the digital focusing error, although this effect obviously significantly contributes to the error in determining the longitudinal coordinates of particles imaged.

The aim of our study is to receive experimental data on the digital focusing error and to compare them with

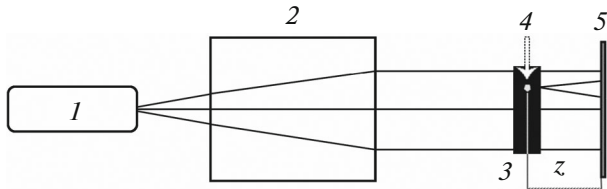


Fig. 1. DHC scheme: coherent radiation source (1); beam expander (2); medium volume to be recorded (sample) (3); particle (defect) (4); detector—CMOS array (5); z is the calculated distance between the hologram recording plane and the plane of best reconstruction of a holographic image.

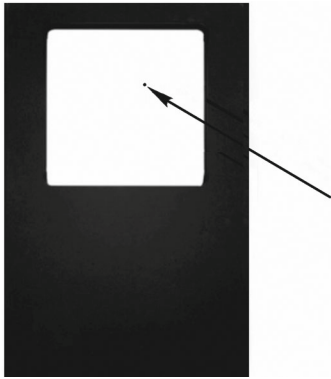


Fig. 2. Model particle deposited on a glass plate (shown by the arrow) fixed in a metal holder.

theoretical estimates of the specklon size for diffraction-limited optical imaging systems.

1. DIGITAL HOLOGRAPHIC CAMERA

An example of an axial scheme of DHC is shown in Fig. 1. Laser diode 1 is used as the source of a reference wave in [4]. It operates in a continuous mode at a wavelength of $1.064 \mu\text{m}$ with average power of 100 mW (a visible laser diode is used in [8]). A light beam of the laser diode is broadened by expander 2. Then the radiation beam with required divergence and diameter falls on test sample 3 (this is a nonlinear crystal with void defects to be diagnosed in [4] and water with plankton particles in [8]). Part of this radiation is scattered by particle 4 and an object wave is generated. A reference wave is generated by the radiation part which has passed through the medium and has not been scattered by particles. The interference pattern of the reference and object waves is recorded in digital form in the computer memory with Baumer VEXG-100M.R. CMOS camera 5. A two-dimensional array of quantized discrete values of the intensity of this interference pattern is a digital hologram.

Holographic images are reconstructed at the distance z by calculating the diffraction integral from the initial hologram intensity distribution, which is

described in detail in [1, 2, 17]. Changing the distance z with a step specified by an operator, the software complex calculates the intensity distribution in different sections of the volume under study and layer by layer forms its virtual 3D image. Images of particles are identified in each reconstructed image of a cross section; their size, shape, orientation, and location inside the volume under study are determined, and real particles are replaced with their digital images (patterns). This is how a digital image of a medium with suspended particles is formed.

In this work, we use a model particle in the form of an opaque square with a side of $500 \mu\text{m}$ as a test object for calibration; it has been photoetched on chromium on a glass substrate; the particle thickness is 200 nm (Fig. 2).

2. TECHNIQUE FOR CALCULATION OF THE LONGITUDINAL SIZE OF A SPECKLON FORMED DURING DIGITAL HOLOGRAM RECORDING AND FOR RECONSTRUCTION OF HOLOGRAPHIC IMAGE

For diffraction-limited optical imaging systems, an image element (pixel) can be represented as a 3D body (cigar, specklon) [16]. The lateral size of this element

$$2\rho = 1.22 \frac{\lambda}{A} \quad (1)$$

and the longitudinal size

$$2\Delta z = \left(\frac{\lambda}{A^2} \right) \approx \frac{(2\rho)^2}{\lambda}, \quad (2)$$

where λ is the wavelength; A is the numerical aperture of the optics system (on the image side) used to imaging.

The numerical aperture of an incoherent optics system is determined by quite specific design parameters: the diameter of the exit pupil of the system D and the distance L from the back principal plane to an image, which are independent of the particle size.

The same is true for DHC. We can write $A = D_h/2L$, where D_h is the diameter of the area occupied by the particle hologram; L is the distance from the hologram to the particle image numerically reconstructed from it. In contrast to an incoherent optics system, D_h depends on the particle size. For example, the area occupied by a hologram of a spherical opaque particle in the far field is the Fraunhofer diffraction pattern on this particle. The sizes of holograms required to reconstruct the image of particles of different shapes are estimated in [7, 17] according to a quality criterion specified. In this interpretation, Equations (1) and (2) allow estimating the dimensions of a specklon in the image space during the reconstruction of the holographic image of the particle (Fig. 3). The corresponding errors in the size and space coordinates of objects (in the volume under study) can be calculated taking

into account the refractive index of the medium where the particles are physically located. For simplicity, the refractive index of the medium where holograms are recorded and reconstructed is assumed to be equal to 1. Thus, Eq. (2) for the DHC system can be rewritten as

$$2\Delta z_h = k_h \left(\frac{\lambda L^2}{D_h^2} \right). \quad (3)$$

Equation (3) is the error in the longitudinal coordinates of an object from the digital hologram; k_h is the empirical coefficient dependent on the focusing method.

As for D_h , the size of the recording array a in a digital holographic system is the aperture maximum limiting the path of radiation beams and the domain of integration in the calculation of the diffraction integral. To record the interference patterns of the reference and object waves, a pixel should be smaller than the period of interference fringes. This depends not only the parameters of the CMOS array of the camera (size of the array, pixel size, total number of pixels), but also on the diffraction region where holograms are recorded, or, in other words, on the distance between a particle and the hologram recording plane.

The conditions required to attain an image quality specified have been studied in [17], where the authors have shown that the required size of the recorded part of the diffraction pattern changes with the particle shape and size and the distance between the particle and the hologram recording plane.

For the DHC technique, we choose a configuration with hologram recording in the Fresnel diffraction region, where the array is the diffraction pattern limiting factor (Fig. 4), which is obviously more than all the possible requirements [17].

Then, taking into account $D_h \approx a$, Eq. (3) is written as

$$2\Delta z_h = k_h \left(\frac{\lambda L^2}{a^2} \right), \quad (4)$$

where $a = 6.44$ mm is the size of the smaller side of the array.

This relation can be used to estimate the possible distances between a particle and the hologram recording plane or to pose restrictions on the length of the volume under study with particles (the depth of the holographic scene).

3. THE ERROR IN THE LONGITUDINAL COORDINATES OF A MODEL PARTICLE UNDER VISUAL FOCUSING

Digital holograms of the test object shown in Fig. 2 and located at different distances L from the photodetector array were recorded following the scheme shown in Fig. 1 for five distances L (Table 1). During the stage of image reconstruction, the distances z in

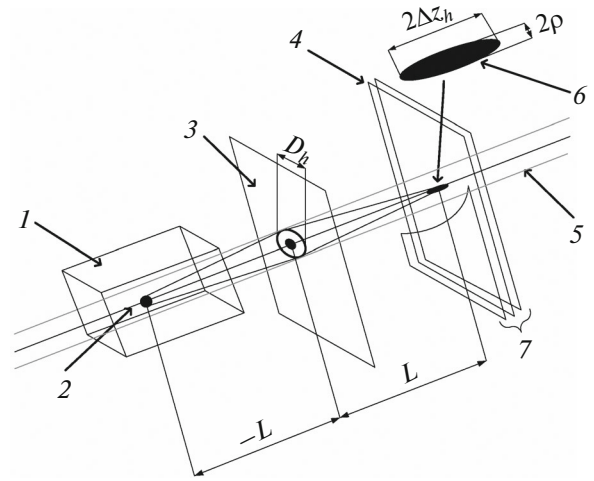


Fig. 3. Digital hologram recording of a particle and reconstruction of its image: medium volume under study (1); particle (2); digital hologram (3); plane of the best reconstruction of the holographic image of the particle (4); recording (real) beam (5); resolution element of the digital holographic system (speckle) (6); set of planes for the analysis and selection of the best image plane composed from the results of numerical reconstruction of the digital hologram (7).

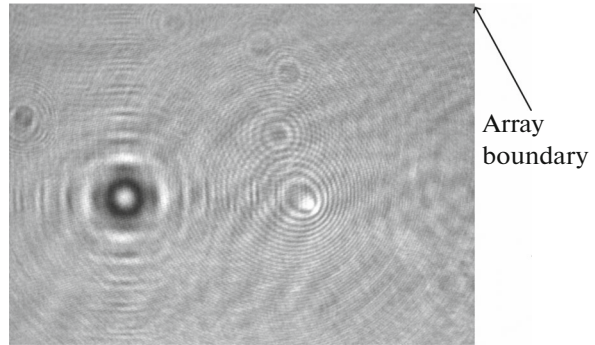
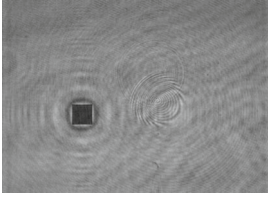
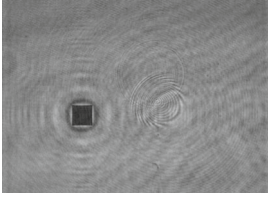
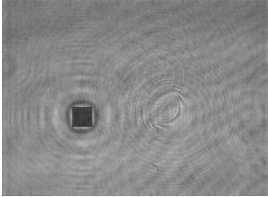
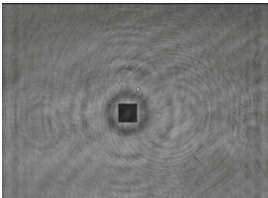
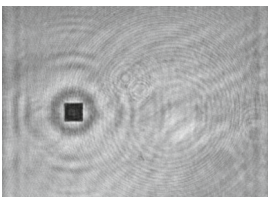


Fig. 4. Hologram of a square particle $500 \times 500 \mu\text{m}$ located at the distance $z = 135$ mm from the recording array with the smaller side size $a = 6.44$ mm.

the diffraction integral are swept with a step of $50 \mu\text{m}$ within the possible location of the image. As a result of calculating the diffraction integral, an array of intensity distributions (hereinafter, reconstructed images) was formed in planes 7 (see Fig. 3), a total of 100 planes for each distance L . The set of the images of cross sections of the volume under study with particles reconstructed from a hologram is constructed in the same way.

The reconstructed images are viewed by an operator which determine the planes of the best image of a model particle (test object), which are visually estimated by the best object sharpness. The sharpness was adjusted 10 times for each of the five holograms. Thus, we have obtained $N = 10$ values of the longitudinal coordinate of the best image plane z_v^i for each hologram.

Table 1. Visual assessments for calculating k_v

k_v	z_v^{av} , mm	$2\Delta z_v$, μm	Δz , μm	L , mm	Model particle in the best image plane
0.16	81.86	114	690	81.7	
0.14	120.69	213	1478	120.5	
0.13	136.6	238	1870	135.5	
0.15	151.4	350	2390	151	
0.17	166.1	485	2828	165.9	

The average value z_v^{av} and the mean square error Δz_v^{av} were calculated for each series of 10 measurements of the longitudinal coordinate of the best image plane by standard methods [18, 19].

To find the confidence interval for the longitudinal coordinate of the best image plane, we used the Student's t -distribution with a confidence level of 95% and $N = 10$:

$$\Delta z_v = 2.3\Delta z_v^{av}. \quad (5)$$

Let us define the correction factor

$$k_v = \frac{2\Delta z_v}{2\Delta z} \quad (6)$$

for visual focusing. Here, $2\Delta z$ is the longitudinal size of a specklon (Eq. (2)) with $D_h \approx a$.

Table 1 shows the visual assessments of the test object for calculating k_v . Based on these data,

$$k_v = 0.15 \pm 0.02. \quad (7)$$

4. THE ERROR IN THE LONGITUDINAL COORDINATES OF A MODEL PARTICLE UNDER DIGITAL FOCUSING

The same array of intensity distributions in planes 7 in Fig. 3, a total of 100 planes for each distance L , was used in the experiment.

The images of model particles reconstructed from the arrays of intensity distributions were digitally processed with the use of such image quality criteria [17, 20–26] as the boundary contrast, boundary brightness jump, and tenengrad.

To calculate the boundary brightness jump and boundary contrast [17, 20, 24], the external (corresponding to the background) and internal (corresponding to the particle image) domains adjacent to this boundary are distinguished along the edge of the reconstructed image of a model particle (Fig. 5), and the average intensities are calculated within these domains. The width of the domains is set to 10% of the size of the particle image. Boundary contrast is defined as

$$K = \frac{\langle I_{IA} \rangle}{\langle I_{EA} \rangle},$$

where $\langle I_{IA} \rangle$ and $\langle I_{EA} \rangle$ are the average intensities in the internal and external domains, respectively.

The boundary brightness jump is calculated as

$$P = \frac{|\langle I_{EA} \rangle - \langle I_{IA} \rangle|}{\langle I \rangle},$$

where $\langle I \rangle$ is the average intensity over the entire image of a cross section (frame) in plane 7 (see Fig. 3).

Tenengrad is the gradient which is measured as the sum of the squares of the responses of the horizontal and vertical Sobel masks

$$S_x(i, j) = \begin{bmatrix} -1 & 0 & 1 \\ -2 & 0 & 2 \\ -1 & 0 & 0 \end{bmatrix} * I(i, j),$$

$$S_y(i, j) = \begin{bmatrix} 1 & 2 & 1 \\ 0 & 0 & 0 \\ -1 & -2 & -1 \end{bmatrix} * I(i, j)$$

($I(i, j)$ is the intensity in the (i, j) image pixel; * is the convolution operation). The tenengrad operator has the form

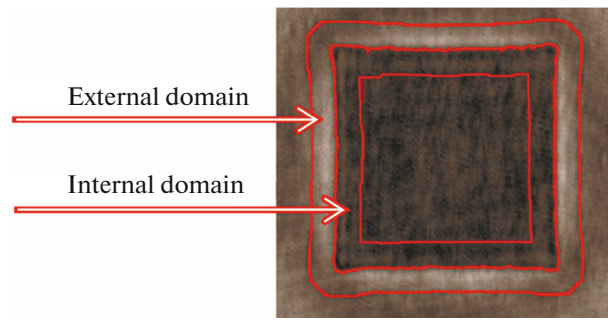


Fig. 5. Internal and external domains in determining a quality criterion.

$$T = \frac{1}{N_x N_y} \sum_{i=0}^{N_x-1} \sum_{j=0}^{N_y-1} G_{i,j},$$

where $G_{i,j} = \sqrt{S_x(i, j)^2 + S_y(i, j)^2}$; N_x, N_y is the number of pixels in the image.

The best image plane is the plane where at least one of the quality criteria (boundary contrast, boundary brightness jump, or tenengrad) attains its maximum. Figure 6 shows the dependences of the selected quality criteria on defocusing and off-tuning (focusing curves) near the point $z = L$, which is the best image plane of a model particle for the same cases as under visual focusing. The focusing curve peaks have a certain width, which can be taken the specklon size (black ellipses).

The digital focusing data are given in Table 2. The processing algorithm allows easy determination of a focusing curve peak and the corresponding coordinate z_d , and it gives an impression of deriving an exact result. However, despite this determinism, it is clearly

Table 2. Focusing curve parameters and digital focusing data

L	Quality criteria	z_d	$z_d - L, \mu\text{m}$	Width of a focusing curve peak at a level of $0.8 \mu\text{m}$ [10]	$2\Delta z, \mu\text{m}$
81.7	Boundary contrast	82.3	600	1600	690
	Boundary brightness jump	81.7	0	200	
	Tenengrad	81.6	-100	200	
120.5	Boundary contrast	120.5	0	500	1478
	Boundary brightness jump	120.9	400	1500	
	Tenengrad	120.6	100	1500	
135.5	Boundary contrast	135.5	0	200	1870
	Boundary brightness jump	135.5	0	200	
	Tenengrad	135.8	300	600	
151	Boundary contrast	151	0	400	2390
	Boundary brightness jump	151	0	800	
	Tenengrad	151.2	200	700	
165.9	Boundary contrast	165	-900	300	2828
	Boundary brightness jump	165	-900	700	
	Tenengrad	165.1	-800	800	

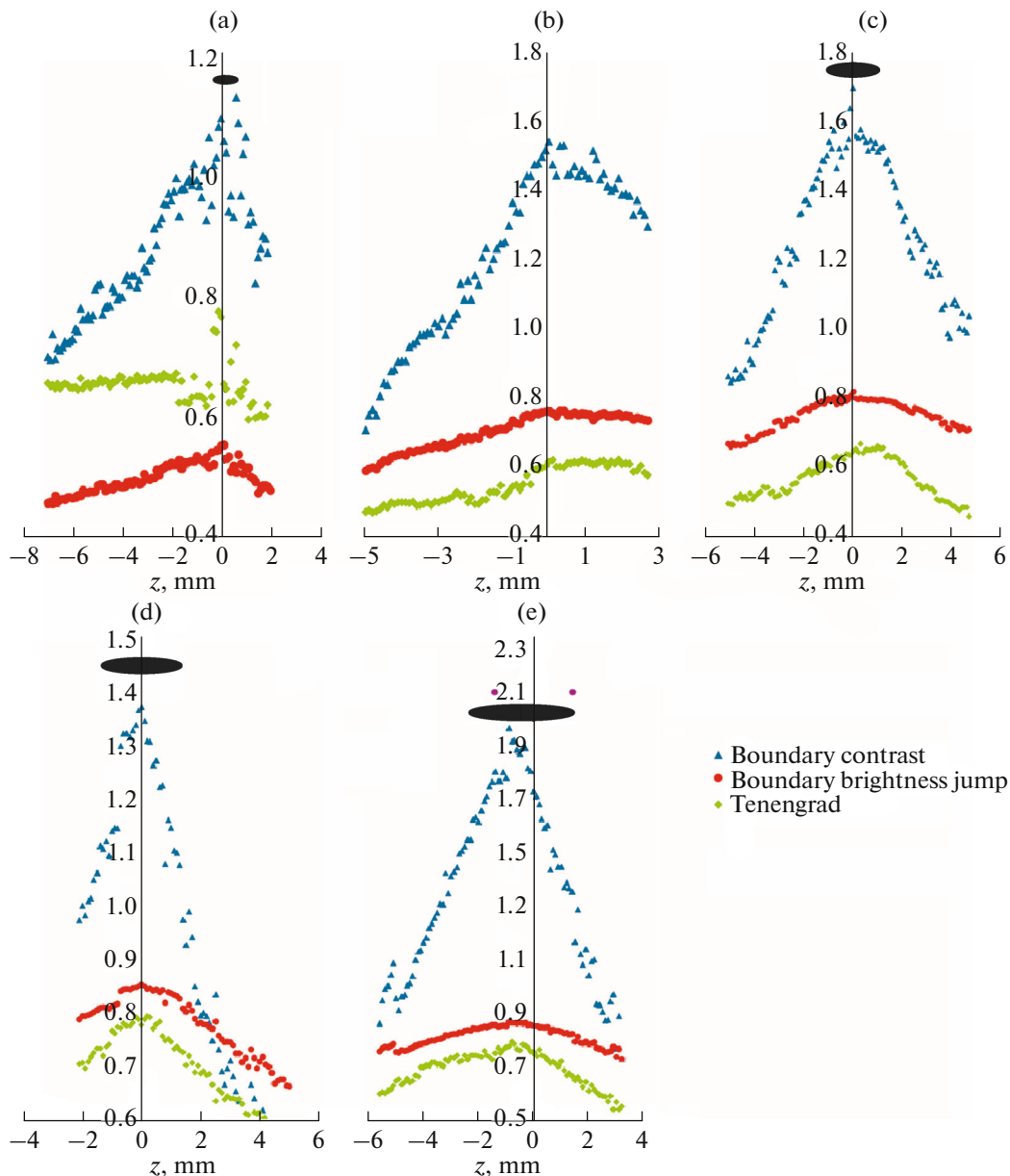


Fig. 6. Autofocusing curves (adjustment to the best image plane) when using different quality criteria for (a) $L = 81.7$, (b) 120.5 , (c) 135.5 , (d) 151 , (e) 165.9 mm. A speckle image corresponding to a distance (Eq. (2) with $D_h \approx a$) is shown at the top.

seen from Fig. 7 that the z_d peaks do not always coincide with each other and with the position of the image L for all considered methods for plotting a focusing curve. Hence, images reconstructed in these planes may be blurred and unsuitable for analysis. The value $2\Delta z_h \approx 2\Delta z$ can be taken as an estimate of the error of this automatic focusing. In accordance with Eq. (4) for single digital focusing, $k_d = 1$ should be taken.

The results confirm that single digital focusing with one image quality criterion cannot compete with visual focusing due to the lack of statistics. Therefore, the accuracy of determining the longitudinal coordinates can be increased by means of extending the sam-

ple of longitudinal readings. A random error can be caused by noise associated with scattering by the medium where the particles are located; the superposition of imaginary and real images, as well as images of closely spaced particles [27]. This is seen in Fig. 7, which shows images reconstructed from full-scale holography and numerical simulation of holography of model hexagonal opaque particles.

One can see distortions in the energy distributions in the domains (internal and external, see Fig. 5) where are quality criteria are calculated induced by distortions associated with scattering by the medium (Fig. 7a) and the superposition of imaginary and real

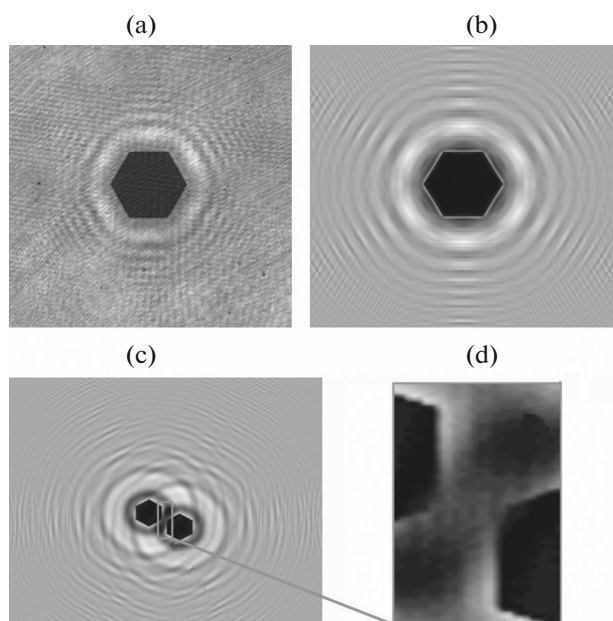


Fig. 7. Holographic images received in (a) the natural experiment with a CMOS camera; numerical simulation of the holography of (b) one and (c) two opaque hexagonal particles in the same plane; the reconstruction distance is 460 mm from the plane.

images typical for the axial scheme (Figs. 7a and 7b), as well as when reconstructing the holographic image of two closely spaced particles. This results in the random error ($z_d - L$) in determining the best image plane by different quality criteria. This error manifests itself in different ways for focusing curves. This emphasizes once again that to increase the accuracy of determining the best image plane (calculating the longitudinal coordinate of a particle), several quality criteria are required.

CONCLUSIONS

Thus, we suggest to use well-known expressions for diffraction-limited optics systems to determine the error in determining the longitudinal coordinates of particles from images reconstructed from digital holograms. The applicability of Eq. (4) to calculation of the possible distances between a particle and the hologram recording plane is shown.

The experiments carried out made it possible to determine the correction factor for visual focusing at different spaces between a particle recorded and the plane of the CMOS array: $k_v = 0.15 \pm 0.02$.

The correction factor $k_v = 1$ for automatic digital focus with one quality criteria of the reconstructed image.

The error of automatic digital focusing can be reduced by the simultaneous use of focusing curves for several quality criteria and optimization of the image region for their construction.

FUNDING

This work was supported by the Russian Science Foundation (grant no. 20-17-00185).

CONFLICT OF INTEREST

The authors declare that they have no conflict of interest.

REFERENCES

1. V. V. Dyomin, A. I. Gribenyukov, A. S. Davydova, M. M. Zinoviev, A. S. Olshukov, S. N. Podzyvalov, I. G. Polovtsev, and N. N. Yudin, "Holography of particles for diagnostics tasks [invited]," *Appl. Opt.* **58** (34), G300–G309 (2019).
2. F. T. S. Yu, *An Introduction To Diffraction, Information Processing, and Holography* (MIT Press, Cambridge, 1973).
3. R. J. Collier, C. B. Burckhardt, and L. H. Lin, *Optical Holography* (Academic, New York, 1971).
4. V. V. Dyomin, A. I. Gribenyukov, S. N. Podzyvalov, N. N. Yudin, M. M. Zinoviev, I. G. Polovtsev, A. Yu. Davydova, and A. S. Olshukov, "Application of infrared digital holography for characterization of inhomogeneities and voluminous defects of single crystals on the example of $ZnGeP_2$," *Appl. Sci.* **10** (2), 442–1 (2020).
5. N. N. Yudin, P. V. Pavlov, M. M. Zinov'ev, S. N. Podzyvalov, V. V. Dyomin, I. G. Polovtsev, I. E. Kuskov, I. E. Vol'f, A. O. Evsin, A. A. Balashov, and A. S. Kostin, "Assessment of fatigue damage of fluoroorganic aircraft glass using digital holography methods," *J. Opt. Technol.* **88** (2), 72–76 (2020).
6. O. Kemppinen, J. C. Laning, R. D. Mersmann, G. Videen, and M. J. Berg, "Imaging atmospheric aerosol particles from a UAV with digital holography," *Sci. Rep.* **10**, 16085 (2020).
7. V. V. Demin, A. S. Olshukov, E. Yu. Naumova, and N. G. Melnik, "Digital holography of plankton," *Atmos. Ocean. Opt.* **21** (12), 951–956 (2008).
8. V. Dyomin, A. Davydova, I. Polovtsev, A. Olshukov, N. Kirillov, and S. Davydov, "Underwater holographic sensor for plankton studies in situ including accompanying measurements," *Sensors* **21** (4863), 1–19 (2021).
9. P. Memmolo, L. Miccio, F. Merola, O. Gennari, P. A. Netti, and P. Ferraro, "3D morphometry of red blood cells by digital holography," *Cytometry A* **85** (12) (2014).
<https://doi.org/10.1002/cyto.a.22570>
10. T. Y. Nikolaeva and N. V. Petrov, "Characterization of particles suspended in a volume of optical medium at high concentrations by coherent image processing," *Opt. Eng.* **54** (8), 083101 (2015).
11. T. A. Vovk and N. V. Petrov, "Correlation characterization of particles in volume based on peak-to-basement ratio," *Sci. Rep.* **7**, 43840 (2017).
12. D. M. Scott, "Recent advances in in-process characterization of suspensions and slurries," *Powder Technol.* **399**, 117159 (2022).

13. S. C. Chapin, V. Germain, and E. R. Dufresne, "Automated trapping, assembly, and sorting with holographic optical tweezers," *Opt. Express* **14**, 13095–13100 (2006).
14. P. J. Rodrigo, R. L. Eriksen, V. R. Daria, and J. Gluckstad, "Interactive light-driven and parallel manipulation of inhomogeneous particles," *Opt. Express* **10**, 1550–1556 (2002).
15. A. V. Bilsky, O. A. Gobysov, and D. M. Markovich, "Evolution and recent trends of particle image velocimetry for an aerodynamic experiment," *Thermophys. Aeromech.* **27** (1), 1–22 (2020).
16. M. Born and E. Wolf, *Principles of Optics* (MIT Press Cambridge: University Press, Cambridge, 1999).
17. V. V. Dyomin and D. V. Kamenev, "Quality criteria for holographic images of particles of various shapes," *Russ. Phys. J.* **53** (9), 927–935 (2011).
18. ISO 2602:1980 "Statistical interpretation of test results—Estimation of the mean—Confidence interval". <https://www.iso.org/standard/7585.html>. Cited 1.09.2022.
19. R. A. Fisher and M. A. Rothamsted, "Statistical methods for research workers," *Metron* **5**, 90 (1925).
20. V. V. Dyomin and D. V. Kamenev, "Evaluation of algorithms for automatic data extraction from digital holographic images of particles," *Russ. Phys. J.* **58** (10), 1467–1474 (2016).
21. W. Huang and Z. Jing, "Evaluation of focus measures in multifocus image fusion," *Pattern Recognit. Lett.* **28** (4), 493–500 (2007).
22. R. C. Gonzalez and R. E. Woods, *Digital Image Processing* (Prentice Hall, New Jersey, 2001).
23. A. Santos, C. Ortiz De Solorzano, J. J. Vaquera, J. M. Pena, N. Malpica, and F. del Pozo, "Evaluation of autofocus functions in molecular cytogenetic analysis," *J. Microsc.* **188** (3), 264–272 (1997).
24. V. V. Dyomin and D. V. Kamenev, "Two-dimensional representation of a digital holographic image of the volume of a medium with particles as a method of depicting and processing information concerning the particles," *J. Opt. Technol.* **80** (7), 450–456 (2013).
25. O. A. Osibote, "Automated focusing in bright-field microscopy for tuberculosis detection," *J. Microsc.* **240** (2), 155–163 (2010).
26. I. V. Vatamanyuk and A. L. Ronzhin, "The use of techniques for estimating the difference in digital images in audiovisual monitoring," *Obrabotka Informatsii Upravlenie* **4**, 16–23 (2014).
27. A. Y. Davydova, V. Dyomin, and I. Polovtsev, "Evaluation of the effect of noise in a digital holographic system on the quality of reconstructed particle image," *Proc. SPIE—Int. Soc. Opt. Eng.* **11560**, 1156020-1 (2020).